

# Active site fingerprinting and pharmacophore screening strategies for the identification of dual inhibitors of protein kinase C (PKC $\beta$ ) and poly (ADP-ribose) polymerase-1 (PARP-1)

Navriti Chadha<sup>1</sup> · Om Silakari<sup>1</sup>

Received: 10 November 2015 / Accepted: 9 May 2016 / Published online: 23 May 2016  
© Springer International Publishing Switzerland 2016

**Abstract** Current clinical studies have revealed that diabetic complications are multifactorial disorders that target two or more pathways. The majority of drugs in clinical trial target aldose reductase and protein kinase C (PKC $\beta$ ), while recent studies disclosed a significant role played by poly (ADP-ribose) polymerase-1 (PARP-1). In light of this, the current study was aimed to identify novel dual inhibitors of PKC $\beta$  and PARP-1 using a pharmaco-informatics methodology. Pharmacophore-based 3D QSAR models for these two targets were generated using HypoGen and used to screen three commercially available chemical databases to identify dual inhibitors of PKC $\beta$  and PARP-1. Overall, 18 hits were obtained from the screening process; the hits were filtered based on their drug-like properties and predicted binding affinities (docking analysis). Important amino acid residues were predicted by developing a fingerprint of the active site using alanine-scanning mutagenesis and molecular dynamics. The stability of the complexes (18 hits with both proteins) and their final binding orientations were investigated using molecular dynamics simulations. Thus, novel hits have been predicted to have good binding affinities for PKC $\beta$  and PARP-1 proteins, which could be further investigated for in vitro/in vivo activity.

**Keywords** PARP inhibitor · PKC $\beta$  inhibitor · Diabetic complications · Molecular dynamics · Quantitative

**Electronic supplementary material** The online version of this article (doi:10.1007/s11030-016-9676-9) contains supplementary material, which is available to authorized users.

✉ Om Silakari  
omsilakari@gmail.com

<sup>1</sup> Molecular Modeling Lab (MML), Department of Pharmaceutical Sciences and Drug Research, Punjab University, Patiala, Punjab 147002, India

structure–activity relationship · Virtual screening · Alanine-scanning mutagenesis

## Introduction

Diabetes mellitus is a metabolic disorder characterized by hyperglycemia, which leads to a number of microvascular abnormalities, such as diabetic nephropathy, retinopathy, and neuropathy, resulting in morbidity, mortality, and deterioration of one's quality of life [1]. Hyperglycemia leads to diabetes-associated anomalies via well-established mechanisms, including increased aldose reductase activity [2], formation of advanced glycation end products (AGEs) [3,4], activation of protein kinase C $\beta$  [5], and hexosamine pathway [6]. In addition, intracellular hyperglycemia causes an increased mitochondrial production of reactive oxygen species (ROS). ROS, in turn, causes DNA strands to break, thereby activating poly (ADP-ribose) polymerase (PARP). PARP reduces the activity of glyceraldehyde-3-phosphate dehydrogenase (GAPDH). Reduced GAPDH activity is involved in activation of the polyol pathway, formation of intracellular AGEs, activation of PKC $\beta$ , and subsequently, nuclear factor  $\kappa$ B (NF $\kappa$ B) and activation of the hexosamine pathway flux [7].

Protein kinase C beta type, encoded by the *PRKCB* gene, is a serine- and threonine-specific protein kinase activated by calcium and diacylglycerol (DAG) and is involved in lipid signaling [5]. Hyperglycemia-induced activation of PKC $\beta$  leads to microvascular abnormalities, such as retinopathy, nephropathy, and neuropathy. Activated PKC $\beta$  may increase retinal endothelial permeability, basement membrane protein synthesis, and stimulates angiogenesis. Ruboxostaurin, a selective PKC $\beta$  inhibitor, has been clinically evaluated to treat diabetic retinopathy

[8]. In the literature, PKC $\beta$  inhibitors with pyrrolopyrazole, *N*-alkylbisindolylmaleimide, macrocyclic bisindolylmaleimide, and balanol, as parent structures, have been reported to manage diabetic complications [9–11].

Poly (ADP-ribose) polymerase (PARP-1), encoded by the *PARP1* gene, is a nuclear enzyme that regulates a number of cellular events, including DNA repair, cellular division and differentiation, DNA replication, transformation, gene expression and amplification, mitochondrial function, and cell death. The altered activity of PARP has been reported in various pathological conditions, including diabetic complications. Experimental data obtained from animal models show that the overexpression of PARP in the retina of diabetic rats occur due to DNA damage induced by cell death [12].

Diabetic complications are a multifactorial disease state; progression is initiated in a number of different pathways (as discussed earlier). Impeding more than one pathway would be a beneficial strategy for ameliorating the disease state. Working on this hypothesis, dual inhibitors of PKC $\beta$  and PARP-1 have been designed to possibly act as benchmarks toward the development of effective therapy in the management of diabetic complications. In this work, based on reported molecules with experimental data, pharmacophore-based 3D-QSAR models have been developed using the HypoGen algorithm [13], which were further validated by the test set prediction, calculation of the enrichment factor (EF), and the goodness of hits (GH) score. The generated pharmacophore models were utilized to screen the commercial Asinex [14], Chembridge [15], and Maybridge databases [16]. The obtained molecules were filtered on the basis of their drug-like properties and docking analysis. Thus, the combined approaches were utilized to obtain compound candidates that can act as potential therapeutic agents to treat diabetic complications.

## Computational methods

### Molecular modeling

For the current study, computational analysis was performed on a Fujitsu Celsius M730 workstation using a NVIDIA Quadro K4000 GPU graphic card and the Linux operating system CentOS 6.5. *Discovery Studio 4.1* software was used to generate HypoGen pharmacophore models [17]. Molecular docking was performed using *CDOCKER* (a CHARMM-based docking tool) [18], and molecular dynamics simulations were carried out using Desmond software (version 3.8) [19–21]. For purposes of performing molecular modeling studies, two proteins were considered: PKC $\beta$  and PARP-1. For PKC $\beta$ , two human-derived structures were available in the Protein Data Bank (PDB): the kinase domain

of PKC $\beta$  protein was available in complex with a bisindolylmaleimide derivative (PDB ID: 2I0E, 2.60 Å), and a full-length structure was available with phosphoaminophosphonic acid adenylate ester (PDB ID: 3PFQ, 4.00 Å) [22]. On the basis of resolution and cross-docking results, the structure with the bisindolylmaleimide derivative (2I0E) was selected for further analysis. On the other hand, for PARP-1, a total of 31 crystallographic structures were available in PDB, for which nine human-derived structures were chosen with a resolution greater than 2.50 Å (Table S1) [23–30]. Based on our cross-docking results, the 2RD6 protein was selected for further analysis. The structures of the proteins were prepared using the automated protein preparation protocol in *Discovery Studio 4.1* (DS). The task to be performed included insertion of missing atoms in the incomplete residues, modeling of missing loops, removal of water, and protonation of titratable residues using predicted pK<sub>s</sub> at a pH value of 7.4 using the CHARMM forcefield.

Selection of training set molecules is critical for the generation of pharmacophore models, which subsequently govern the quality of the generated model. PKC $\beta$  and PARP-1 inhibitors reported in the literature with experimental inhibitory activities (reported as IC<sub>50</sub> values) were selected as the training set [31–41]. The training set molecules had diverse chemical structures, and their activities spanned more than 4 orders of magnitude. The protonation states of all the molecules were obtained using the *Prepare Ligands* protocol in DS (pH 6.5–7.5), and the molecular geometry of the resulting compounds was calculated using the CHARMM forcefield.

### Pharmacophore analysis and validation

A pharmacophore hypothesis was generated using DS in which a pharmacophore is defined as an ensemble of essential chemical features or substructures and their corresponding three-dimensional positions, which are responsible for the molecular recognition of a ligand by a specific biological target to trigger (or block) its biological response. Pharmacophore-based 3D-QSAR analyses for PKC $\beta$  and PARP-1 inhibitors (based on the Catalyst *HypoGen* algorithm) were carried out by considering the hydrogen bond donor, hydrogen bond acceptor, hydrophobic, ring aromatic, and positive/negative ionizable features on the ligand [13,17]. For this analysis, a training set of 23 and 31 molecules were selected for PKC $\beta$  and PARP-1, respectively, on the basis of their structural diversity and variation in activity. The activities of these compounds were classified as highly active, moderately active, and inactive. A maximum of 255 conformations were generated for each ligand using “BEST conformation generation,” and an energy threshold of 20 kcal/mol was considered to ensure maximum coverage

of the conformational space. A total of 10 pharmacophore models were generated by taking six maximum and four minimum features. To assess the significance of the generated pharmacophore models, a Fischer's randomization test with 95 % confidence limits was used. While generating the hypothesis, the minimum and maximum counts of features for hydrogen bond acceptor (HBA), hydrogen bond donor (HBD), hydrophobic feature (HY), positive ionizable (PI), negative ionizable (NI), and aromatic ring (RA), were set as 0 and 5, respectively, for each feature type. This protocol led to the generation of a total of 10 quantitative hypotheses with their corresponding statistical parameters, including cost values (null and fixed costs), correlation ( $R^2$ ), the root mean square deviation (RMSD), and fit values. Fixed cost represents the simplest model that fits the data perfectly. Null cost represents the highest cost of pharmacophore with no features and estimates the activity to be the average of the activity of the training set compounds. The best model was selected on the basis of the difference between two cost values (null cost minus total cost). A model with a difference greater than 60 means that the model has a true correlation; a difference of 40–60 indicates a prediction correlation of 70–90 %, and a difference below 40 reflects difficulty in prediction.

The best pharmacophore model is able to differentiate active from inactive molecules. Selected pharmacophore models were assessed using the Fischer's method, and their validation was carried forth using the test set molecules. The Fischer's method assesses the correlation between chemical structure and biological activity and overrules the probability of chance correlation. Test set was utilized to determine the ability of the hypothesis to predict the molecules and categorize them according to their range of biological activities. The prediction was carried out in DS using the BEST algorithm and Flexible fitting option.

The generated hypotheses were further validated using calculation of the enrichment factor (EF) and Goodness of hits (GH) [42]. The enrichment factor (EF) was calculated to check the ability of the models to predict the active molecules over the inactives (decoys) using the formula:  $EF = (H_a/H_t)/(A/D)$ , while the goodness of hits was assessed by screening the model through a database of known actives and inactives and the results were evaluated using the Güner-Henry (GH) scoring method based on the following equation:

$$GH = \{[H_a \times (3A + H_t)] / 4H_t A\} \times \{(H_t - H_a) / (D - A)\}$$

where D is the total number of compounds in the database, A is the number of actives,  $H_a$  is the total number of actives on the hit list, and  $H_t$  is the total number of compounds on the hit list. The calculated GH scores range from 0 (null model) to 1 (ideal model).

## Docking and molecular dynamics simulation

All the docking simulations were carried out using the *CDOCKER* module in *DS 4.1* [18], which works on the CHARMM-based forcefield, and molecular dynamics simulations in the *Desmond* software, which works on the OPLS\_2005 forcefield [19–21]. All the reported PKC $\beta$  and PARP-1 inhibitors were docked in the prepared PKC $\beta$  protein (PDB: 2I0E) and PARP-1 protein (PDB: 2RD6), respectively. The results were analyzed for the presence of hydrogen bonding, hydrophobic and  $\pi$ – $\pi$  interactions between molecules, and the active site of the proteins.

The molecule with the highest target affinity for each class of reported inhibitors docked with the PKC $\beta$  and PARP-1 proteins was used in molecular dynamics simulations (10 ns) using Desmond. The simulations helped to stabilize the complex and analyze the most probable interaction by studying its simulation–interaction diagram. From this analysis, the important interactions for each prototypic ligand were assessed and can be utilized for further designing.

For molecular dynamics simulations, the system was first built using the TIP3P solvent model with orthorhombic box shape; the pH was adjusted by adding Na<sup>+</sup> ions, and the salt concentration was set at 0.15 M. The simulation was carried out using the NPT ensemble and a time step of 1.0 fs; the temperature was fixed at 310K using the Nose-Hoover Chain method as the thermostat and pressure of 1.01325 bar using Martyn–Tobias–Klein as the barostat.

## Alanine-scanning mutagenesis

Alanine-scanning mutagenesis is a method that systematically substitutes residues with alanine for the identification of functional epitopes. This alanine substitution removes all the side chain atoms after the  $\beta$ -carbon; thus, the role of side chain functional groups at a particular position can be assessed from alanine mutations. In the present work, a computational alanine scanning mutagenesis was carried out, wherein *Binding Mutational Energy* was calculated using *DS* under the Macromolecules toolbar [17]. In this protocol, the energy effect of each mutation on the binding affinity (mutational energy,  $\Delta\Delta G_{mut}$ ) was calculated as the difference between the binding free energy in mutated and wild-type protein [ $\Delta\Delta G_{mut} = \Delta\Delta G_{bind}(mutant) - \Delta\Delta G_{bind}(wildtype)$ ]. Alanine scanning for all amino acid residues of the active site of PKC $\beta$  and PARP-1 was performed.

Based on the results obtained from the molecular dynamics simulation and alanine-scanning mutagenesis, various amino acids present in the active site were ranked based on their participation in binding the inhibitor at the active site.

The scores obtained from the simulation and mutation analyses were used as markers for the current study.

### Virtual screening protocol

The process of virtual screening is the most critical step in the theoretical process; thus, we combined a ligand-based and structure-based approaches to obtain better results. A ligand-based approach, i.e., pharmacophore screening, helps to obtain features common in all of the highest active molecules included in the dataset, while the structure-based approach, i.e., docking analysis helps to obtain molecules that can potentially have the best interaction with the PKC $\beta$  and PARP-1 protein. A hierarchical virtual screening protocol was followed to screen the commercially available Asinex, Chembridge, and Maybridge databases consisting of 296,321, 49,962, and 54,262 molecules, respectively, using

the *Flexi search method* in DS by PKC $\beta$  and PARP-1 pharmacophore models in a stepwise fashion. This led to the retrieval of hits that fit all of the features of the selected pharmacophore model. The obtained hits were filtered based on Lipinski's rule of five, where a drug could be absorbed when it has less than 10 hydrogen bond acceptors, less than five hydrogen bond donor groups, a molecular weight of less than 500 Da, and the number of rotatable bonds is less than 10.

The calculation of absorption, distribution, metabolism, excretion, and toxicity (ADMET) properties was carried out using the *ADMET Descriptor* protocol in DS. Various parameters calculated in this process include human intestinal absorption (HIA), aqueous solubility, blood–brain barrier penetration (BBB), cytochrome P4502D6 (CYP2D6) enzyme inhibition, and hepatotoxicity. Human intestinal absorption is calculated on the basis of a model developed using descriptors, including AlogP98 and 2D polar surface area (PSA\_2D) [43, 44]. The absorption is ranked in four pre-

**Table 1** Cost analysis and correlation data for the pharmacophore hypothesis of PARP-1

Hypothesis	Total cost	Error cost	RMS	Correlation ( <i>R</i> )	Feature
Hypo1	100.83	82.91	1.08	0.93	HBA, HY, PI, RA
Hypo2	101.82	84.39	1.14	0.93	HBA, HBA, HY, PI
Hypo3	107.33	92.26	1.42	0.88	HBA, HBA, HY, PI
Hypo4	109.23	94.49	1.48	0.87	HBA, HY, HY, PI
Hypo5	109.32	94.54	1.47	0.87	HBA, HY, PI, RA
Hypo6	110.81	95.86	1.54	0.86	HBA, HY, HY, PI
Hypo7	110.94	95.82	1.54	0.86	HBA, HBA, HY, PI
Hypo8	114.87	99.48	1.66	0.84	HBA, HY, HY, PI
Hypo9	116.51	101.53	1.71	0.83	HBA, HY, HY, PI
Hypo10	120.53	105.31	1.82	0.80	HBA, HBA, PI, RA

Null cost = 169.89, Fixed cost = 85.29, Configuration cost = 13.67, All costs are in units of bits.

All pharmacophores consist of four features including hydrogen-bond acceptor (HBA), hydrogen-bond donor (HBD), hydrophobic (HY), polarizable (P), and aromatic ring (RA)

**Table 2** Cost analysis and correlation data for the pharmacophore hypothesis of PKC $\beta$

Hypothesis	Total cost	Error cost	RMS	Correlation ( <i>R</i> )	Feature
Hypo-1	92.58	75.63	1.11	0.89	HBA, HBA, HBD, HY
Hypo2	93.44	77.52	1.19	0.87	HY, HY, PI, RA
Hypo3	94.09	78.09	1.22	0.87	HY, HY, PI, RA
Hypo4	95.00	78.51	1.22	0.87	HBA, HBA, HBD, HY
Hypo5	97.21	80.78	1.29	0.85	HBA, HBD, HY, PI
Hypo6	97.83	81.69	1.38	0.83	HY, HY, RA, RA
Hypo7	98.56	82.54	1.38	0.83	HBA, HBD, HY, PI
Hypo8	98.62	82.34	1.40	0.82	HY, HY, HY, RA
Hypo9	99.03	83.03	1.42	0.82	HBD, HY, PI, RA
Hypo10	99.27	83.37	1.42	0.82	HY, HY, PI, RA

Null cost = 122.89, Fixed cost = 79.66, Configuration cost = 14.74, All costs are in units of bits.

All pharmacophores consist of four features including hydrogen-bond acceptor (HBA), hydrogen-bond donor (HBD), hydrophobic (HY), polarizable (P), and aromatic ring (RA)

diction levels: 0, 1, 2, and 4, referring to good, moderate, low, and very low absorption, respectively. Aqueous solubility is calculated using a predictive model for aqueous solubility [43], and ranking for the same is denoted as 0, 1, 2, 3, 4, or 5, corresponding to extremely low, very low, low, good, optimal, or very soluble profile of compounds, respectively. The blood–brain barrier penetration is also calculated using a quantitative regression model [45], where the 0, 1, 2, 3, and 4 values correspond to very high, high, medium, low, and undefined penetration. Based on a Bayesian model, a compound could be predicted as a CYP2D6 inhibitor or hepatotoxic [46–48].

Compounds fulfilling the criteria of drug-likeness were chosen for molecular docking studies using *CDOCKER* as discussed above. Selected molecules were docked against PKC $\beta$  (PDB ID: 2IOE) and PARP-1 (PDB ID: 2RD6), and the interactions were evaluated with the fingerprint residues of the protein that were extracted as mentioned earlier. The final hits were further simulated for 10 ns to assess their stability at the active sites of PKC $\beta$  and PARP-1.

## Results and discussion

As per our design strategy, we first sketched and prepared the ligand molecules identified in the literature known to be PKC $\beta$  and PARP-1 inhibitors. A total of 23 PKC $\beta$  and 31 PARP-1 inhibitors were identified with experimental IC<sub>50</sub> values. Using the selected training set molecules, the 3D-QSAR pharmacophore analysis was carried out, and a total of 10 hypotheses were generated. The top hypothesis consisted of four features: hydrogen bond acceptor (HBA), hydrophobic (HY), positively ionizable (PI), and ring aromatic (RA) for both PKC $\beta$  and PARP-1. The results of the cost analysis and correlation of the pharmacophore hypothesis for PARP-1 and PKC $\beta$  are shown in Tables 1 and 2, respectively. The best Hypo-1 hypothesis from each pharmacophoric hypothesis was selected for further investigation based on statistical results. The value of the total cost was closer to the fixed-cost value, which is required for a good hypothesis. For PKC $\beta$  and PARP-1, the difference between the null cost hypothesis and fixed-cost hypothesis was found to be 43.23 and 84.6 bits, respectively. The values of the null-cost hypothesis and total cost of the best models of PKC $\beta$  and PARP-1 were found to be 122.89 and 92.58 bits, and 169.89 and 100.83 bits, respectively. The correlation between the experimental and estimated activities of the training set compounds yielded correlation coefficient ( $R^2$ ) values of 0.89 and 0.93 for PKC $\beta$  and PARP-1, respectively (Fig. 1). The pharmacophores of both models mapped well onto the highest active molecules with good fitness scores of 9.5 and 9.3 for PKC $\beta$  and PARP-1, respectively. The estimated activities of the training set compounds obtained from Hypo1 of PKC $\beta$  and

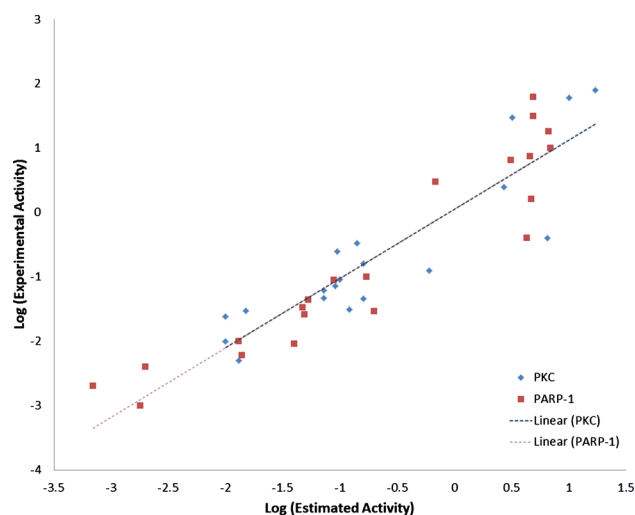


**Fig. 1** Correlation between experimental and estimated activities of training set compounds of Hypo 1 of PKC $\beta$  (blue) and PARP-1 (maroon). (Color figure online)

PARP-1 are shown in Tables S2 and S3, respectively. Similarly, for test set compounds, estimated activities are given in Tables S4 and S5. Important features identified in both the pharmacophore models follow binding interactions of the active molecules docked within the PKC $\beta$  and PARP-1 active site. The hypothesis selected for PKC $\beta$  consists of two acceptors: one donor and one hydrophobic group (Fig. 2a). Superimposition of the hypothesis over the highest active molecule (PKC-J, Supplementary Table S2) suggested that the two acceptors and one donor group lie over the carbonyls and NH moiety of maleimide of the molecule, respectively (Fig. 2b). In our docking analysis, these groups, i.e., the two carbonyls and NH moieties were involved in the hydrogen-bond formation with Thr404, Glu421, and Val423 amino acids. In addition, the hydrophobic group lies over the methyl group, which fits into the small hydrophobic pocket of the active site. The hypothesis selected for PARP-1 consists of one acceptor, one hydrophobic, one aromatic ring, and one positively polarizable feature (Fig. 2c). It is evident from Fig. 2d that the acceptor feature lies over the carbonyl of the amide group of the highest active molecule (PARP-1, Supplementary Table S3); the hydrophobic feature lies over the indazole ring; the aromatic ring feature lies over the phenyl group; and the positive polarizable feature lies over the NH of the molecule (Fig. 2d). The amide group formed hydrogen-bond interactions with Gly202 and Ser243, the indazole ring forms  $\pi$ – $\pi$  interactions with Tyr246, while the positive ionizable NH lies in the solvent-accessible area and improves the solubility profile of the molecule.

For the validation of the pharmacophore models, a test set of 8 and 15 known PKC $\beta$  and PARP-1 inhibitors were identified and categorized as active, inactive, and moder-



**Fig. 2** The best pharmacophore model Hypo 1 of a PKC $\beta$  contains two hydrogen bond acceptors (HBA: *green*), one hydrogen bond donor (HBD: *magenta*), and one hydrophobic (HY: *blue*). b Alignment of Hypo 1 of PKC $\beta$  over the most active compound. c PARP-1 contains one hydrogen bond acceptor (HBA: *green*), one hydrogen bond donor (HBD: *magenta*), one aromatic ring (RA: *orange*), and one hydrophobic (HY: *blue*). d Alignment of Hypo 1 of PARP-1 over the most active compound. (Color figure online)

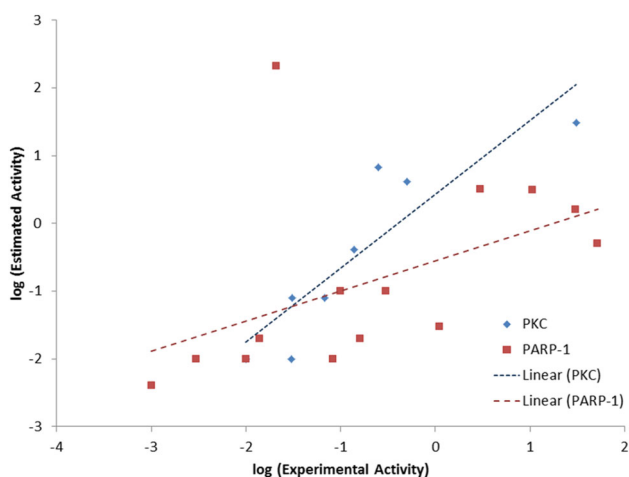
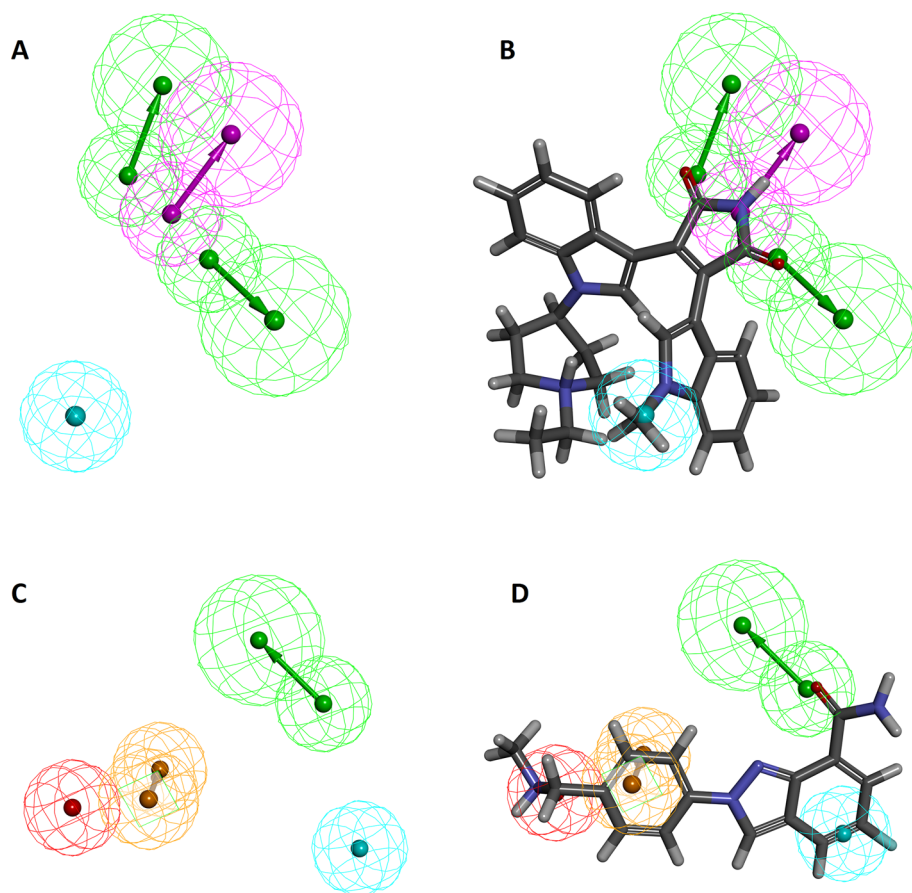


**Fig. 3** Correlation between experimental and estimated activities of test set compounds of Hypo 1 of PKC $\beta$  (*blue*) and PARP-1 (*maroon*). (Color figure online)

ately active. The selected hypotheses for both targets were able to predict the test set molecules according to their activity range and displayed  $q^2$  values of 0.63 and 0.76 for PKC $\beta$  and PARP-1, respectively. The selected hypotheses also showed good correlation between the experimental

and estimated activity (Fig. 3). Thus, the test set validation results demonstrated that the hypotheses can discriminate between actives, moderately actives, and inactive. Further validation of the pharmacophore model was carried out by screening a database of 56 and 222 known PKC $\beta$  and PARP-1 inhibitors, respectively, consisting of 26 and 156 actives ( $IC_{50} \leq 100$  nM), and 30 and 66 inactive ( $IC_{50} \geq 1$   $\mu$ M) molecules, respectively, which were screened through their respective pharmacophore models. Moderately active molecules ( $IC_{50} = 100$  nM to  $1$   $\mu$ M) were not considered in the database to differentiate between the actives and inactive. The PKC $\beta$  and PARP-1 pharmacophore models gave an enrichment value of 1.77 and 1.19, respectively (Supplementary Table S6). A GH score of 0.69 and 0.49 for PKC $\beta$  and PARP-1, respectively, indicates the models are of significant good quality.

In order to improve the selectivity of the design process, a structure-based design approach was incorporated into the protocol. For this reason, the protein of PKC $\beta$  (PDB ID: 2I0E) was selected on the basis of resolution and cross-docking results. The protein was first prepared to correct any missing hydrogen atoms, ambiguous protonation states, and flapped residues. Then, all the dataset molecules were docked at the active site of the prepared protein. The docking

results showed good correlation between the experimental activity and *CDOCKER* interaction energy, with a correlation coefficient value of 0.65 (Supplementary Fig. S1). Thus, the crystal structure 2IOE was used and the protein's chain A was selected on the basis of the *B*-value for further analysis. Furthermore, the protein-ligand complexes of the most potent active molecules from each series were simulated for a period of 10 ns to establish the stability of the compound's interactions with the amino acid residues. Our simulation showed that meleimide of co-crystal ligand interacts with the hinge region amino acids Glu421, Val423, and Thr404 (Supplementary Fig. S2A). The NH of the ring acted as a hydrogen bond donor to the backbone carbonyl of Glu421 amino acid residue, while the carbonyls of the ring formed a hydrogen bond interaction with Thr404 and Val423. Further analysis revealed that hydrophobic interactions with Phe353, Val356, and Ala483 also played a key role in ligand binding (Supplementary Fig. S2B). Similarly, the macrocyclic bisindolylmaleimides parent structure containing clinical trial molecule ruboxostaurin formed hydrogen-bonding interactions with Glu421 and Val423 (Supplementary Fig. S3). In addition, hydrophobic interactions were observed with Phe353, Ala483, Met473, Ala369, and Val356. The PKC $\beta$  inhibitor with pyrrolopyrazole scaffold (PKC-9, Supplementary Table S2) formed three hydrogen-bonding interactions, i.e., NH of pyrazole with Glu421, nitrogen of pyrazole with Val423 and NH of the amide group on 3rd position of pyrrolopyrazole ring with Val423 of the PKC $\beta$  active site (Supplementary Fig. S4). PKC-9 also formed hydrophobic interactions with amino acid residues Phe353 and Val356 (Supplementary Fig. S5). Information regarding contacts of the ligands with amino acid residues was obtained in the form of an interaction fraction value that helped to rank the amino acids in the order of their importance.

In the case of PARP-1, out of a total of nine available PDB structures and based on cross-docking analysis, the crystal structure 2RD6 was selected and prepared for further analysis. All the molecules were docked in the protein and the *CDOCKER* interaction energy was correlated with experimental activity with a correlation coefficient of 0.55 (Supplementary Fig. S6). The critical analysis of all available crystal structures with inhibitor molecules suggested the presence of some common interactions that may be considered important for inhibiting the PARP-1 protein. The major interactions assessed from the available crystal structures are mentioned in Supplementary Table S7. Based on our results, we determined that interactions with amino acid residues Gly202 and Ser243 are essential for activity, aromatic amino acid residues Tyr246 and His201 formed  $\pi$ - $\pi$  interactions with the aromatic ring system of the inhibitor and Lys242 is involved in  $\pi$ -cation interaction in some of the crystal complexes.

The information obtained from molecular dynamics simulations is not sufficient to rank the active site amino acid residues. Thus, an alanine-scanning mutagenesis was carried out to rank the amino acid residues at the active site. For this, mutational energies were calculated by mutating different amino acid residues with alanine. The mutational energies were calculated to evaluate the effect of mutations on the binding affinity of ligands in protein-ligand complexes. We performed combinatorial alanine-scanning mutagenesis on a set of selected amino acid residues by mutating them to alanine. The energy effect of each mutation on the binding affinity (mutational energy) was calculated as the difference between binding free energy in the mutated structure and wild protein:  $\Delta\Delta G_{\text{mut}} = \Delta\Delta G_{\text{bind}}(\text{mutant}) - \Delta\Delta G_{\text{bind}}(\text{wild type})$ . The binding free energy ( $\Delta\Delta G_{\text{bind}}$ ) refers to the difference between the free energies of the protein-ligand complex and protein in an unbound state. All the respective calculations were performed using the CHARMM forcefield and Generalized Born implicit water model. In this calculation, an empirical summation of electrostatic interaction, Van der Waal interaction, entropy contribution of changes in side-chain mobility, and a nonpolar surface-dependent contribution to solvation energy was designated as the total energy. The results obtained from the single point alanine mutagenesis can be scaled according to its values, mutational energy less than  $-0.5$  kcal/mol is referred to as stabilizing, mutational energy between  $-0.5$  and  $0.5$  kcal/mol is described as neutral, and mutational energy greater than  $0.5$  kcal/mol is destabilizing. The alanine-scanning mutagenesis was carried out for the active site amino acid residues, taking ligands with different scaffolds. The mutational energies obtained for each amino acid residue of the active site of PKC $\beta$  and PARP-1 from this scanning are summarized in Supplementary Tables S8 and S9, respectively.

The information obtained from the simulation studies and alanine scanning mutagenesis helped to rank the different amino acids in the PKC $\beta$  and PARP-1 active sites and develop fingerprint of active sites of these two targets (Tables 3, 4).

In the PKC $\beta$  active site, the amino acid residues Glu421, Val423, and Thr404 present in the hinge region turn out to be important in simulation studies. It was observed that amino acids Leu348, Phe353, and Val356 form a hydrophobic groove on the roof of the active site, where the hydrophobic group of inhibitor can be well accommodated. A small groove was also present at the bottom of the active site, formed by Met473 and Ala483 amino acid residues. These hydrophobic grooves are also crucial because the amino acid residues constituting the groove are ranked high in the above analyses. The edge of the active site consists of acidic amino acids Asp427, Asp470, Asp484, and Glu390, which are observed to line the active site and interact with the positively charged group in the inhibitor molecule. The back of the active site is lined up with hydrophobic residues, such as Met420 and

**Table 3** Ranking of active site amino acid residues of PKC $\beta$  by molecular dynamics simulation and alanine scanning mutagenesis

Amino acid	Rank	Reason
Glu421	1	Constitute hinge region interaction (simulation study)
Val423	2	Constitute hinge region interaction (simulation study)
Phe353	3	Form hydrophobic interaction (simulation and computational mutagenesis)
Thr404	4	Constitute hinge region interaction (simulation study)
Val356	5	Form hydrophobic interaction (simulation and computational mutagenesis)
Met473	6	Form hydrophobic interaction (simulation and computational mutagenesis)
Leu348	7	Form hydrophobic interaction (simulation and computational mutagenesis)
Tyr422	8	As calculated from simulation and mutagenesis score
Asp484	9	As calculated from simulation and mutagenesis score
Asp470	10	As calculated from simulation and mutagenesis score
Met420	11	As calculated from simulation and mutagenesis score
Lys371	12	As calculated from simulation and mutagenesis score
Glu390	13	As calculated from simulation and mutagenesis score

**Table 4** Ranking of active site amino acid residues of PARP-1 by Crystal structure scrutinization and alanine-scanning mutagenesis

Amino acid	Rank	Reason
Gly202	1	Crystal structure scrutinization
Ser243	2	Crystal structure scrutinization
Tyr246	3	Crystal structure scrutinization and computational mutagenesis
Tyr235	4	Crystal structure scrutinization and computational mutagenesis
His 201	5	Crystal structure scrutinization and computational mutagenesis
Lys242	6	Crystal structure scrutinization and computational mutagenesis
Tyr228	7	Crystal structure scrutinization and computational mutagenesis
Glu327	8	Computational mutagenesis
Glu102	9	Computational mutagenesis

Ala369. The amino acid residues Lys371 and Glu390 form a salt-bridge interaction and act as gatekeeper residues in the active site. Furthermore, based on interactions of the reported crystal structures for PARP-1, molecular dynamics simulation, and mutational analysis, amino acids of the active site were ranked, as shown in Table 5. Thus, a fingerprint of the PARP-1 active site was developed: Gly202 and Ser243 are important amino acids that form backbone acceptor–donor interactions with the inhibitor; the amino acids His201, Tyr235, Ala237, and Tyr228 line the base of the active site; and Lys242 and Tyr246, which present at the roof of the active site, are involved in forming  $\pi$ – $\pi$  and  $\pi$ -cation interaction. The acidic amino acid Glu327, present at the edge of the active site, was observed to form an interaction with the positively-charged entity in the inhibitor.

A hierarchical virtual screening protocol was utilized, as shown in Fig. 4. The pharmacophoric features of the selected hypothesis play a critical role in screening out novel hits from commercially available chemical databases. The pharmacophore hypothesis of PKC $\beta$  mapped 194,995, 28,295, and 23,796 molecules from the Asinex, Chembridge, and Maybridge databases, respectively, while screening from the

pharmacophore hypothesis of PARP-1 led to retrieval of 19,169, 8511, and 713 hits, respectively. The hits were first filtered on the basis of their fitness scores: compounds with fit values greater than 8.5 and 7.5 were considered for PKC $\beta$  and PARP-1, respectively. These hits from the PKC $\beta$  and PARP-1 screening were filtered using the Lipinski's and ADMET filter. In order to calculate the pharmacokinetic profile of the hits, the ADMET properties were calculated, such as blood–brain barrier (BBB) penetration, solubility, hepatotoxicity, human intestinal adsorption (HIA), and CYP450 2D6 inhibition. For BBB, solubility, and absorption, compounds with values of 3, 3, and 0 were assigned to low penetration, good aqueous solubility, and low absorption, respectively. Additionally, based on Bayesian model the hits were predicted as CYP2D6 inhibitor and nonhepatotoxic.

The hits obtained from the PKC $\beta$  screening were subsequently cross-screened through PARP-1 and vice versa to obtain dual inhibitors. Hits from cross-screening process were combined and docked against PKC $\beta$  (PDB ID: 2I0E) and PARP-1 (PDB ID: 2RD6) and evaluated for their binding orientations within the active site. The whole process yielded a total of 18 potential dual inhibitors with a purine-



**Table 5** 2D- Structures of hits screened from Anisex database along with estimated activities of PKC $\beta$  and PARP-1

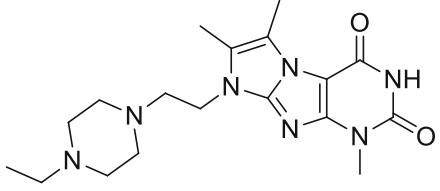
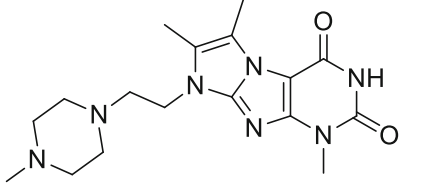
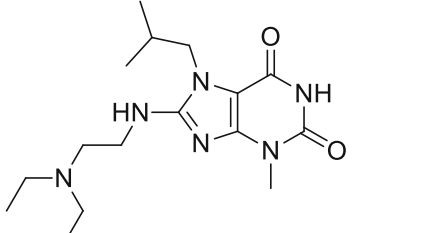
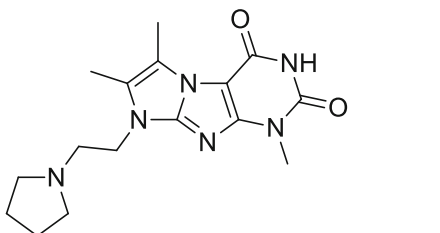
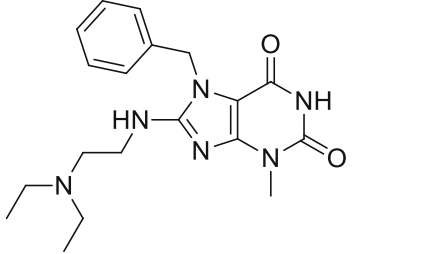
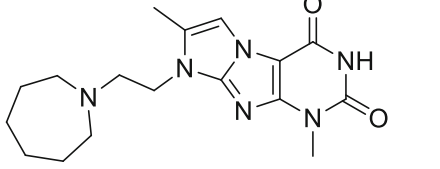
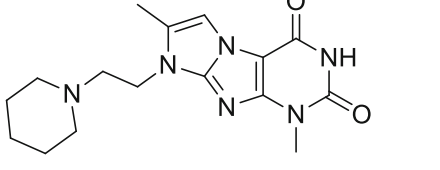
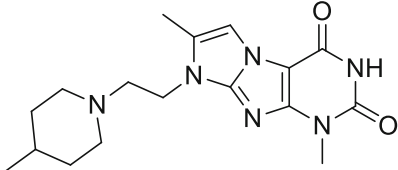
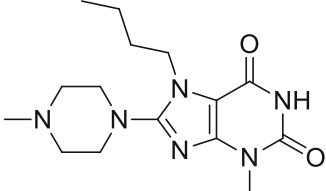
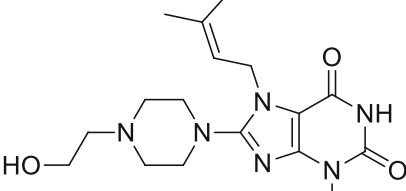
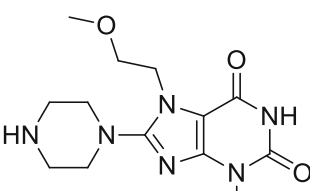
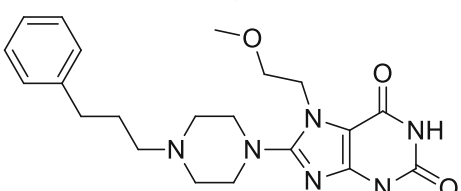
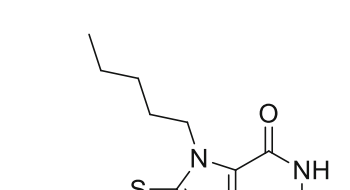
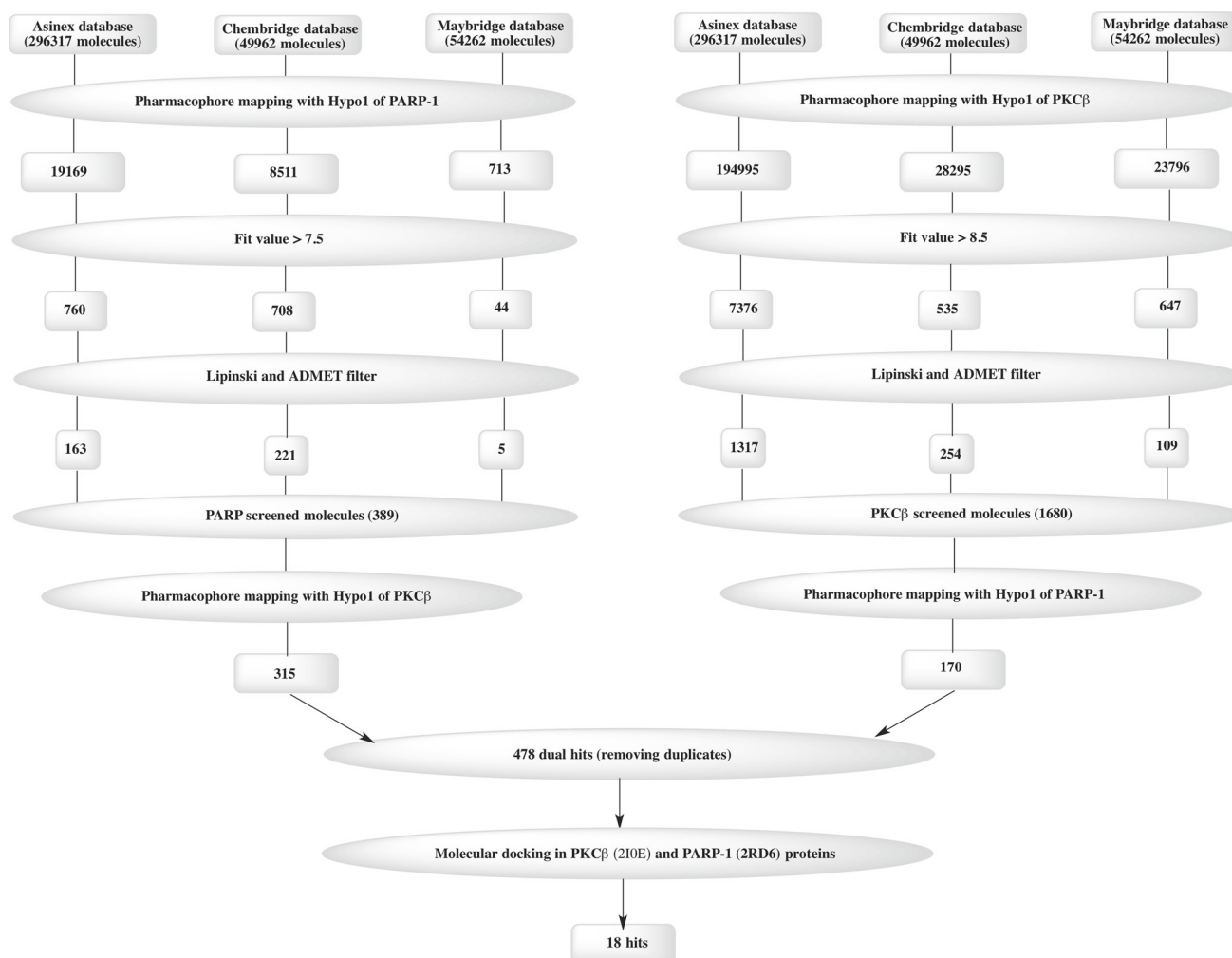
Code	Structure	Estimated activity PKC $\beta$	Estimated Activity PARP-1	MM-GBSA (PKC $\beta$ )	MM-GBSA (PARP-1)
BAS17260509		8.9	3.5	-72.26	-92.63
BAS17260501		9.04	1.97	-72.20	-90.68
BAS02999118		8.78	5.05	-72.05	-66.37
ASN17260521		8.5	1.82	-70.50	-85.65
ASN00387070		9.00	3.42	-68.41	-67.55
BAS17260446		8.51	1.26	-70.50	-90.92
BAS17260422		8.52	1.68	-66.77	-85.54

Table 5 continued

Code	Structure	Estimated activity PKC $\beta$	Estimated Activity PARP-1	MM-GBSA (PKC $\beta$ )	MM-GBSA (PARP-1)
BAS17260425		9.06	1.45	-66.63	-88.04
BAS01122536		9.14	1.46	-66.41	-85.48
BAS06502901		8.54	1.01	-65.33	-104.94
BAS13765774		9.02	2.5	-65.33	-91.26
BAS13117570		8.57	6.5	-63.74	-81.79
BAS04914706		9.03	3.09	-63.58	-97.82

**Table 5** continued

Code	Structure	Estimated activity PKC $\beta$	Estimated Activity PARP-1	MM-GBSA (PKC $\beta$ )	MM-GBSA (PARP-1)
BAS04914704		9.09	2.39	-61.70	-96.40
BAS07401527		9.03	2.03	-60.53	-95.04
BAS17260444		8.9	4.4	-60.40	-83.78
BAS13117571		8.63	6.27	-57.10	-87.31
BAS02999084		8.72	6.5	-48.83	-72.38



**Fig. 4** Virtual screening protocol followed to identify 18 potential dual-target hit molecules

2,6-dione scaffold (Table 5). The best molecules mapped over the PKC $\beta$  and PARP-1 pharmacophore models are shown in Supplementary Figs. S5A and B. Finally, a molecular dynamics simulation was used to assess the binding stability of the obtained hits with the respective protein targets. Thus, all the complexes, i.e., Asinex molecules in complex with PKC $\beta$  and PARP-1 proteins, were subjected to MD simulations for a period of 10 ns. To analyze stability of the protein-ligand complexes, the RMSD values of protein backbone and hit compounds were calculated; they ranged from 0.5 to 3.5 Å for proteins and 0.8 to 4.3 Å for the ligands. The graph of the root mean square deviation (RMSD) values for the best molecule simulated with PKC $\beta$  and PARP-1 are shown in Supplementary Figs. S7A and S7B, respectively. Variations in RMSD, noted during the initial intervals, were due to an initial adjustment of the hits into the active site of the respective proteins. However, ligands showed stability after initial adjustment in terms of RMSD, as well as interactions within the active site. All structures superimposed onto the reference

ligand showed a similar binding pose. The hit-1 with a purine-2,6-dione substructure showed hydrogen-bond interactions with the hinge region amino acids Thr404, Glu421, and Val423 of PKC $\beta$  protein (Fig. 5c). In addition, hit-1 showed hydrophobic interactions with Ala369 and Ala483. These interactions were found to be stable throughout a molecular dynamics simulation period of 10 ns. Hit-1 also displayed stable hydrogen-bond interactions with Gly202 and Ser243 at the PARP-1 active site (Fig. 5d). It also formed a stable  $\pi$ - $\pi$  interaction with Tyr246 and hydrophobic contacts with Tyr228 and Tyr235 amino acid residues. Because the hit compounds showed good interactions within the active sites of both proteins, the final hits can be considered promising candidates as potential dual inhibitors of PKC $\beta$  and PARP-1.

The binding energies of the complexes between identified hits and PKC $\beta$  and PARP-1 proteins were also calculated using the MM-GBSA method to determine the relative affinity of the obtained hits (Table 5). The binding energies of the PKC $\beta$ -ligand complex were  $-90.69$  kcal/mol (PKC-



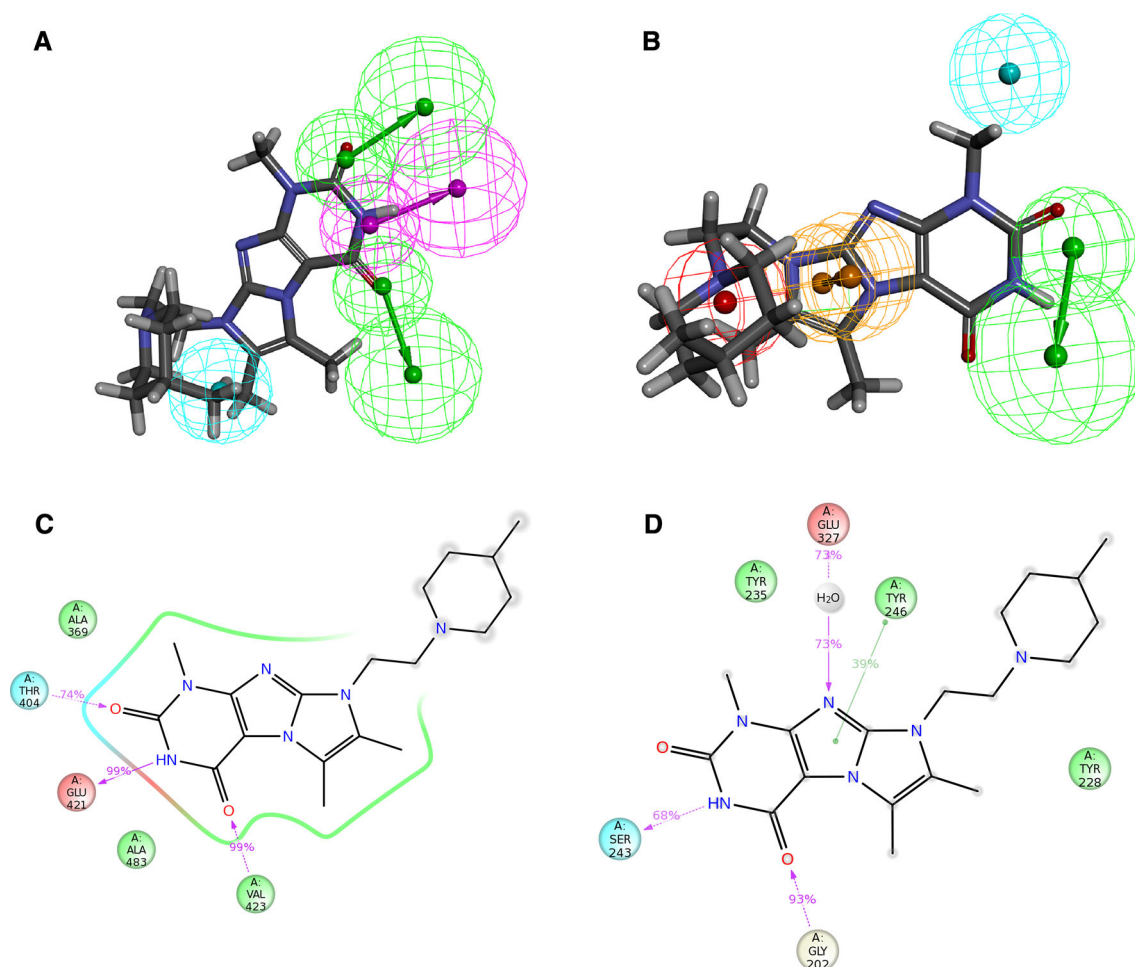


**Fig. 5** Final best-hit compound mapped onto the best pharmacophore model of **a** PKC $\beta$ , **b** PARP-1. The HBA, HBD, RA, and HY features are displayed in *green, magenta, orange* and *cyan*, respectively. Docking interaction of the best-hit compound with proteins of **c** PKC $\beta$ , **d** PARP-1. (Color figure online)

hit1), while for the PARP-1-ligand complex it was  $-72.26$  kcal/mol (PARP-hit1). In addition, it was checked whether these compounds had earlier been evaluated for PKC $\beta$  and PARP-1 inhibitory activities or not using *PubChem Structure* online search tool (September, 2015, <https://pubchem.ncbi.nlm.nih.gov/>). This search confirmed that the hits were not experimentally tested earlier for the inhibition of PKC $\beta$  and PARP-1. These results concluded that the final hits could provide a potential architecture for designing novel dual inhibitors of PKC $\beta$  and PARP-1.

## Conclusion

In recent years, rigorous work has been done to develop appropriate therapeutic agents for diabetic complications. Activation of multiple pathways related to the disease leads to therapy complications. Thus, in our present work, we aimed to identify dual inhibitors of two well-established

targets of diabetic complications: PKC $\beta$  and PARP-1. For this, rigorously validated pharmacophore models were developed for PKC $\beta$  and PARP-1 inhibitors, and these pharmacophore models were utilized for virtual screening. To improve the sensitivity and specificity of the process, docking analysis was carried out, which helped to determine key interactions and key amino acids at the active site. A hierarchical virtual screening approach was used to identify dual inhibitors of PKC $\beta$  and PARP-1 that may be utilized as potential agents for the treatment of diabetic complications.

**Acknowledgments** The authors thank the Council for Scientific and Industrial Research (CSIR), New Delhi for providing the financial support (No. 02(0111)/12/EMR-II).

**Author Contribution** Navriti Chadha designed, performed the study and wrote the paper; Dr. Om Silakari supervised the project.

## References

- Fowler MJ (2008) Microvascular and macrovascular complications of diabetes. *Clin Diabetes* 26:77–82. doi:10.2337/diaclin.26.2.77
- Chung SS1, Ho EC, Lam KS, Chung SK (2003) Contribution of polyol pathway to diabetes-induced oxidative stress. *J Am Soc Nephrol* 14:S233–S236. doi:10.1097/01.ASN.0000077408.15865.06
- Giardino I, Edelstein D, Brownlee M (1994) Nonenzymatic glycosylation in vitro and in bovine endothelial cells alters basic fibroblast growth factor activity. A model for intracellular glycosylation in diabetes. *J Clin Invest* 94:110. doi:10.1172/JCI117296
- Horie K, Miyata T, Maeda K, Miyata S, Sugiyama S, Sakai H, van Ypersele de Strihou C, Monnier VM, Witztum JL, Kurokawa K (1997) Immunohistochemical colocalization of glycoxidation products and lipid peroxidation products in diabetic renal glomerular lesions. Implication for glycoxidative stress in the pathogenesis of diabetic nephropathy. *J Clin Invest* 100:2995–3004. doi:10.1172/JCI119853
- Xia P, Kramer RM, King GL (1995) Identification of the mechanism for the inhibition of Na<sup>+</sup>, K<sup>+</sup> (+)-adenosine triphosphatase by hyperglycemia involving activation of protein kinase C and cytosolic phospholipase A2. *J Clin Invest* 96:733. doi:10.1172/JCI118117
- Sayeski PP, Kudlow JE (1996) Glucose metabolism to glucosamine is necessary for glucose stimulation of transforming growth factor- $\alpha$  gene transcription. *J Biol Chem* 271:15237–15243. doi:10.1074/jbc.271.25.15237
- Brownlee M (2005) The pathobiology of diabetic complications: a unifying mechanism. *Diabetes* 54:1615–1625. doi:10.2337/diabetes.54.6.1615
- Clarke M, Dodson PM (2007) PKC inhibition and diabetic microvascular complications. *Best Pract Res Clin Endocrinol Metab* 21:573–586. doi:10.1016/j.beem.2007.09.007
- Faul MM, Gillig JR, Jirousek MR, Ballas LM, Schotten T, Kahl A, Mohr M (2003) Acyclic N-(azacycloalkyl)bisindolylmaleimides: isozyme selective inhibitors of PKC $\beta$ . *Bioorg Med Chem Lett* 13:1857–1859. doi:10.1016/S0960-894X(03)00286-5
- Hu H, Mendoza JS, Lowden CT, Ballas LM, Janzen WP (1997) Synthesis and protein kinase C inhibitory activities of balanol analogues with modification of 4-hydroxybenzamide moiety. *Bioorg Med Chem* 5:1873–1882. doi:10.1016/S0968-0896(97)00125-9
- Li H, Hong Y, Nukui S, Lou J, Johnson S, Scales S, Botrous I, Tompkins E, Yin C, Zhou R, He M, Jensen J, Bouzida D, Alton G, Lafontaine J, Grant S (2011) Identification of novel pyrrolopyrazoles as protein kinase C  $\beta$  II inhibitors. *Bioorg Med Chem Lett* 21:584–587. doi:10.1016/j.bmcl.2010.10.032
- Mohammad G, Siddiquei MM, Abu El-Asrar AM (2013) Poly (ADP-Ribose) polymerase mediates diabetes-induced retinal neuropathy. *Mediators Inflamm* 2013:510451. doi:10.1155/2013/510451
- Li H, Sutter J, Hoffmann R (2000) HypoGen: an automated system for generating predictive 3D pharmacophore models. In: Güner OF (ed) *Pharmacophore perception, development, and use in drug design*. International University Line, La Jolla, CA, pp 173–189
- Asinex Gold Platinum database. <http://www.asinex.com/>. Accessed Sep 2015
- Chembridge database. <http://www.chembridge.com/index.php>. Accessed Aug 2015
- Maybridge database. <http://www.maybridge.com/>. Accessed Aug 2015
- Discovery Studio version 4.1, (2015) Accelrys Inc., San Diego, CA. [www.accelrys.com](http://www.accelrys.com)
- Wu G, Robertson DH, Brooks CL, Vieth M (2003) Detailed analysis of grid-based molecular docking: a case study of CDOCKER-A CHARMM-based MD docking algorithm. *J Comput Chem* 24:1549–1562. doi:10.1002/jcc.10306
- Bowers KJ, Chow E, Xu H, Dror RO, Eastwood MP, Gregersen B, Klepeis JL, Kolossvary I, Moraes MA, Sacerdoti FD, Salmon JK, Shan Y, Shaw DE (2006) Scalable algorithms for molecular dynamics simulations on commodity clusters. *SC 2006 Conference, Proceedings of the ACM/IEEE*. IEEE 84: 43–43. doi:10.1145/1188455.1188544
- Guo Z, Mohanty U, Noehre J, Sawyer TK, Sherman W, Krilov G (2010) Probing the  $\alpha$ -helical structural stability of stapled p53 peptides: molecular dynamics simulations and analysis. *Chem Biol Drug Des* 75:348–359. doi:10.1111/j.1747-0285.2010.00951.x
- Shivakumar D, Williams J, Wu Y, Damm W, Shelley J, Sherman W (2010) Prediction of absolute solvation free energies using molecular dynamics free energy perturbation and the OPLS force field. *J Chem Theory Comput* 6:1509–1519. doi:10.1021/ct900587b
- Leonard TA, Rózycki B, Saidi LF, Hummer G, Hurley JH (2011) Crystal structure and allosteric activation of protein kinase C  $\beta$ II. *Cell* 144:55–66. doi:10.1016/j.cell.2010.12.013
- Aoyagi-Scharber M, Gardberg AS, Yip BK, Wang B, Shen Y, Fitzpatrick PA (2014) Structural basis for the inhibition of poly (ADP-ribose) polymerases 1 and 2 by BMN 673, a potent inhibitor derived from dihydropyridophthalazinone. *Acta Crystallogr F Struct Biol Commun* 70:1143–1149. doi:10.1107/S2053230X14015088
- Gangloff AR, Brown J, De Jong R, Dougan DR, Grimshaw CE, Hixon M, Jennings A, Kamran R, Kiryanov A, O'Connell S, Taylor E, Vu P (2013) Discovery of novel benzo [b][1, 4] oxazin-3 (4H)-ones as poly (ADP-ribose) polymerase inhibitors. *Bioorg Med Chem Lett* 23:4501–4505. doi:10.1016/j.bmcl.2013.06.055
- Ye N, Chen C-H, Chen T, Song Z, He JX, Huan XJ, Song SS, Liu Q, Chen Y, Ding J, Xu Y, Miao ZH, Zhang A (2013) Design, synthesis, and biological evaluation of a series of benzo [de][1, 7] naphthyridin-7 (8 H)-ones bearing a functionalized longer chain appendage as novel PARP1 inhibitors. *J Med Chem* 56:2885–2903. doi:10.1021/jm301825t
- Penning TD, Zhu G-D, Gong J, Thomas S, Gandhi VB, Liu X, Shi Y, Klinghofer V, Johnson EF, Park CH, Fry EH, Donawho CK, Frost DJ, Buchanan FG, Bukofzer GT, Rodriguez LE, Bontcheva-Diaz V, Bouska JJ, Osterling DJ, Olson AM, Marsh KC, Luo Y, Giranda VL (2010) Optimization of phenyl-substituted benzimidazole carboxamide poly (ADP-ribose) polymerase inhibitors: identification of (S)-2-(2-fluoro-4-(pyrrolidin-2-yl) phenyl)-1 H-benzimidazole-4-carboxamide (A-966492), a highly potent and efficacious inhibitor. *J Med Chem* 53:3142–3153. doi:10.1021/jm901775y
- <http://www.rcsb.org/pdb/explore/explore.do?structureId=3gn7>. Accessed April 2015
- Miyashiro J, Woods KW, Park CH, Liu X, Shi Y, Johnson EF, Bouska JJ, Olson AM, Luo Y, Fry EH, Giranda VL, Penning TD (2009) Synthesis and SAR of novel tricyclic quinoxalinone inhibitors of poly (ADP-ribose) polymerase-1 (PARP-1). *Bioorg Med Chem Lett* 19(15):4050–4054. doi:10.1016/j.bmcl.2009.06.016
- <http://www.rcsb.org/pdb/explore/explore.do?structureId=2rd6>. Accessed April 2015
- Ferraris D, Ficco RP, Pahutski T, Lautar S, Huang S, Zhang J, Kalish V (2003) Design and synthesis of poly (ADP-ribose) polymerase-1 (PARP-1) inhibitors. Part 3: in vitro evaluation of 1, 3, 4, 5-tetrahydro-benzo [c][1, 6]-and [c][1, 7]-naphthyridin-6-ones. *Bioorg Med Chem Lett* 13(15):2513–2518. doi:10.1016/S0960-894X(03)00465-7
- Jagtap PG, Southan GJ, Baloglu E, Ram S, Mabley JG, Marton A, Salzman A, Szabó C (2004) The discovery and synthesis of novel adenosine substituted 2, 3-dihydro-1H-isoindol-1-ones: potent inhibitors of poly (ADP-ribose) polymerase-1 (PARP-1). *Bioorg Med Chem Lett* 14:81–85. doi:10.1016/j.bmcl.2003.10.007

32. Ishida J, Hattori K, Yamamoto H, Iwashita A, Mihara K, Matsuoka N (2005) 4-Phenyl-1, 2, 3, 6-tetrahydropyridine, an excellent fragment to improve the potency of PARP-1 inhibitors. *Bioorg Med Chem Lett* 15:4221–4225. doi:[10.1016/j.bmcl.2005.06.094](https://doi.org/10.1016/j.bmcl.2005.06.094)
33. Ishida J, Yamamoto H, Kido Y, Kamijo K, Murano K, Miyake H, Ohkubo M, Kinoshita T, Warizaya M, Iwashita A, Mihara K, Matsuoka N, Hattori K (2006) Discovery of potent and selective PARP-1 and PARP-2 inhibitors: SBDD analysis via a combination of X-ray structural study and homology modeling. *Bioorg Med Chem Lett* 14:1378–1390. doi:[10.1016/j.bmcl.2005.09.061](https://doi.org/10.1016/j.bmcl.2005.09.061)
34. Chen J, Peng H, He J, Huan X, Miao Z, Yang C (2014) Synthesis of isoquinolinone-based tricycles as novel poly (ADP-ribose) polymerase-1 (PARP-1) inhibitors. *Bioorg Med Chem Lett* 24:2669–2673. doi:[10.1016/j.bmcl.2014.04.061](https://doi.org/10.1016/j.bmcl.2014.04.061)
35. Hattori K, Kido Y, Yamamoto H, Ishida J, Kamijo K, Murano K, Ohkubo M, Kinoshita T, Iwashita A, Mihara K, Yamazaki S, Matsuoka N, Teramura Y, Miyake H (2004) Rational approaches to discovery of orally active and brain-penetrable quinazolinone inhibitors of poly (ADP-ribose) polymerase. *J Med Chem* 47:4151–4154. doi:[10.1021/jm0499256](https://doi.org/10.1021/jm0499256)
36. Jones P, Altamura S, Boueres J, Ferrigno F, Fonsi M, Giomini C, Lamartina S, Montegudo E, Ontoria JM, Orsale MV, Palumbi MC, Pesci S, Roscilli G, Scarpelli R, Schultz-Fademrecht C, Toniatti C, Rowley M (2009) Discovery of 2-4-[(3 S)-Piperidin-3-yl] phenyl-2 H-indazole-7-carboxamide (MK-4827): a novel oral poly (ADP-ribose) polymerase (PARP) Inhibitor efficacious in BRCA-1 and-2 mutant tumors. *J Med Chem* 52:7170–7185. doi:[10.1021/jm901188v](https://doi.org/10.1021/jm901188v)
37. Lord A-M, Mahon MF, Lloyd MD, Threadgill MD (2008) Design, synthesis, and evaluation in vitro of quinoline-8-carboxamides, a new class of poly (adenosine-diphosphate-ribose) polymerase-1 (PARP-1) inhibitor. *J Med Chem* 52:868–877. doi:[10.1021/jm8013629](https://doi.org/10.1021/jm8013629)
38. Menear KA, Adcock C, Boulter R, X-1 Cockcroft, Copsey L, Cranston A, Dillon KJ, Drzewiecki J, Garman S, Gomez S, Javaid H, Kerrigan F, Knights C, Lau A, Loh VM Jr, Matthews IT, Moore S, O'Connor MJ, Smith GC, Martin NM (2008) 4-[3-(4-cyclopropanecarbonylpiperazine-1-carbonyl)-4-fluorobenzyl]-2 H-phthalazin-1-one: a novel bioavailable inhibitor of poly (ADP-ribose) polymerase-1. *J Med Chem* 51:6581–6591. doi:[10.1021/jm8001263](https://doi.org/10.1021/jm8001263)
39. Orvieto F, Branca D, Giomini C, Jones P, Koch U, Ontoria JM, Palumbi MC, Rowley M, Toniatti C, Muraglia E (2009) Identification of substituted pyrazolo [1, 5-a] quinazolin-5 (4H)-one as potent poly (ADP-ribose) polymerase-1 (PARP-1) inhibitors. *Bioorg Med Chem Lett* 19:4196–4200. doi:[10.1016/j.bmcl.2009.05.113](https://doi.org/10.1016/j.bmcl.2009.05.113)
40. Scarpelli R, Boueres JK, Cerretani M, Ferrigno F, Ontoria JM, Rowley M, Schultz-Fademrecht C, Toniatti C, Jones P (2010) Synthesis and biological evaluation of substituted 2-phenyl-2H-indazole-7-carboxamides as potent poly (ADP-ribose) polymerase (PARP) inhibitors. *Bioorg Med Chem Lett* 20:488–492. doi:[10.1016/j.bmcl.2009.11.127](https://doi.org/10.1016/j.bmcl.2009.11.127)
41. Sunderland PT, Woon EC, Dhama A, Bergin AB, Mahon MF, Wood PJ, Jones LA, Tully SR, Lloyd MD, Thompson AS, Javaid H, Martin NM, Threadgill MD (2011) 5-Benzamidoisoquinolin-1-ones and 5-( $\omega$ -carboxyalkyl) isoquinolin-1-ones as isoform-selective inhibitors of poly (ADP-ribose) polymerase 2 (PARP-2). *J Med Chem* 54:2049–2059. doi:[10.1021/jm1010918](https://doi.org/10.1021/jm1010918)
42. Jasuja H, Chadha N, Kaur M, Silakari O (2014) Dual inhibitors of Janus kinase 2 and 3 (JAK2/3): designing by pharmacophore- and docking-based virtual screening approach. *Mol Divers* 18:253–267. doi:[10.1007/s11030-013-9497-z](https://doi.org/10.1007/s11030-013-9497-z)
43. Egan WJ, Lauri G (2002) Prediction of intestinal permeability. *Adv Drug Deliv Rev* 54:273–289. doi:[10.1016/S0169-409X\(02\)00004-2](https://doi.org/10.1016/S0169-409X(02)00004-2)
44. Egan WJ, Merz KM, Baldwin JJ (2000) Prediction of drug absorption using multivariate statistics. *J Med Chem* 43:3867–3877. doi:[10.1021/jm000292e](https://doi.org/10.1021/jm000292e)
45. Cheng A, Merz KM (2003) Prediction of aqueous solubility of a diverse set of compounds using quantitative structure-property relationships. *J Med Chem* 46:3572–3580. doi:[10.1021/ci9501507](https://doi.org/10.1021/ci9501507)
46. Susnow RG, Dixon SL (2003) Use of robust classification techniques for the prediction of human cytochrome P450 2D6 inhibition. *J Chem Inf Comput Sci* 43:1308–1315. doi:[10.1021/ci030283p](https://doi.org/10.1021/ci030283p)
47. Xia X, Maliski EG, Gallant P, Rogers D (2004) Classification of kinase inhibitors using a Bayesian model. *J Med Chem* 47:4463–4470. doi:[10.1021/jm0303195](https://doi.org/10.1021/jm0303195)
48. Cheng A, Dixon SL (2003) In silico models for the prediction of dose-dependent human hepatotoxicity. *J Comput Aid Mol Des* 17:811–823. doi:[10.1023/B:JCAM.0000021834.50768.c6](https://doi.org/10.1023/B:JCAM.0000021834.50768.c6)